Chapter 2
Anodization: A Promising Nano Modification Technique of Titanium-Based Implants for Orthopedic Applications

T.J. Webster and C. Yao

Abstract Titanium is protected by a thin titanium oxide layer, which spontaneously forms on its surface when exposed to air or other oxygen-containing environments. This oxide passive layer is typically 2–5 nm thick and is responsible for the well-documented corrosion resistance property of titanium and its alloys. Because of this and their excellent mechanical properties, titanium and its alloys are widely used in orthopedic and dental applications. However, the native TiO_2 layer is not bioactive enough to form a direct bonding with bone, which means the lack of osseointegration to juxtaposed bone might lead to long-term failure after implantation. Specifically, the 10- to 15-year lifetime of current titanium-based orthopedic implants is not as long as expected by many patients. This chapter reviews many of the current research that is being carried out to extend the life of implants by nano modification techniques.

2.1 Introduction

Many attempts have been made to improve the surface properties of titanium-based implants (e.g., topography, chemistry, and surface energy), which directly determine the implant-environment interactions after implantation [1–3]. These surface modification techniques include mechanical methods (e.g., sand-blasting), chemical methods (e.g. acid etching), coatings (e.g., plasma spraying), etc. [4–9]. Through these conventional approaches, a better bonding ability with bone has been achieved due to the creation of a optimum microscale surface roughness, a more favorable surface chemistry, and/or a new morphology preferred by bone-forming cells (or osteoblasts). However, neither these mechanical nor chemical methods

T.J. Webster (✉) · C. Yao
Brown University, Providence, RI, USA
e-mail: Thomas_webster@brown.edu

W. Ahmed and M.J. Jackson (eds.), *Surgical Tools and Medical Devices*,
DOI 10.1007/978-3-319-33489-9_2

have the ability to produce controlled surface topographies. Moreover, these methods have the potential to form surface residuals. Thus, alternative methods to modify titanium surfaces are highly desirable for promoting new bone growth.

Other attempts to improve bone-bonding involves coating titanium-based implants with hydroxyapatite (HA) or other calcium phosphates, which is commonly accomplished by plasma spraying [2]. This is based on the fact that HA and other calcium phosphates are the main inorganic components of bone and they have been shown by many to directly bond to juxtaposed bone [10–13]. Unfortunately, such coatings have long-term failures due to weak adhesion to the metal substrate and dissolution once implanted. Therefore, an alternative method to deposit HA firmly onto titanium surfaces with optimal bioactivity is highly desirable for orthopedic applications.

In this light, a current strategy is to modify titanium-based implants to possess nanometer surface features considering that natural bone is a nanostructured material. It is important to note that type I collagen (organic matrix of bone) is a triple helix 300 nm in length, 0.5 nm in width, and periodicity of 67 nm while HA (inorganic mineral phase of bone) are approximately 20–40 nm long. Besides, HA crystals are uniquely patterned within the collagen network [14]. These indicate that bone cells may be used to an environment in nanoscale rather than microscale. Recently, human osteoblasts were observed to initially adhere to grain boundaries on both nanophase and conventional titanium; greater osteoblast adhesion was found on nanophase titanium that possessed more grain boundaries on the surface [15]. However, the mechanical strength of this nanophase titanium (compacts of nanoparticles) was not high enough for use as a bulk material like titanium alloys through metallurgy techniques. Proper nanometer surface modification methods for current titanium-based implants are, thus, being actively pursued.

An electrochemical method known as anodization or anodic oxidation is a well-established surface modification technique for valve metals to produce protective layers [4]. It has been successfully used as a surface treatment for orthopedic implants in the past few decades and it has some new advances recently. This chapter will present an overview of anodization and discuss processing parameters, microstructure and composition, biological responses of anodized titanium, which are pertinent for orthopedic applications. Finally, this chapter will also discuss mechanisms of enhanced osteoblast functions on anodized titanium that possesses nanometer structures.

2.2 Anodization of Titanium

2.2.1 Basics of Anodization Process

Typical anodization procedures include alkaline cleaning, acid activation, and electrolyte anodizing. Acid activation is performed in a mixture of nitric acid and

hydrofluoric acid (HF) to remove the natural titanium oxide layer and surface contaminants. The electrolyte anodization is carried out in an electrochemical cell, which usually has a three-electrode configuration (titanium anode, platinum cathode, and Ag/AgCl reference electrode). When a constant voltage or current is applied between the anode and cathode, electrode reactions (oxidation and reduction) in combination of field-driven ion diffusion lead to the formation of an oxide layer on the anode surface.

The main chemical reactions specifically for anodizing titanium are listed below (Eq. (2.1)–(2.5) adapted from [4]).

At the Ti/Ti oxide interface:

$$\mathrm{Ti} \Leftrightarrow \mathrm{Ti}^{2+} + 2e^{-} \tag{2.1}$$

At the Ti oxide/electrolyte interface:

$$2\mathrm{H_2O} \Leftrightarrow 2\mathrm{O}^{2-} + 4\mathrm{H}^{+} \tag{2.2}$$

$$2\mathrm{H_2O} \Leftrightarrow \mathrm{O_2} + 4\mathrm{H}^{+} + 4e^{-} \tag{2.3}$$

At both interfaces:

$$\mathrm{Ti}^{2+} + 2\mathrm{O}^{2-} \Leftrightarrow \mathrm{TiO_2} + 2e^{-} \tag{2.4}$$

Because titanium oxides have higher resistivity than the electrolyte and the metallic substrate, the applied voltage will mainly drop over the oxide film on the anode. As long as the electrical field is strong enough to drive the ion conduction through the oxide, the oxide film will keep growing. This explains why the final oxide thickness, d, is almost linearly dependent on the applied voltage, U:

$$d \approx aU \tag{2.5}$$

where a is usually a constant within the range 1.5–3 nm/V [4].

2.2.2 *Influences of Processing Parameters*

The resulting oxide film properties (such as degree of nanometer roughness, morphology, chemistry, etc.) after anodization varies over a wide range according to different process parameters such as applied potential (voltage), current density, electrolyte composition, pH, and temperature. Different acids (phosphoric acid-H_3PO_4, sulfuric acid-H_2SO_4, acetic acid-CH_3COOH, and others), neutral salts, and alkaline solutions are widely used electrolytes for the anodization of titanium. Their detailed electrochemical oxide growth behavior on titanium was studied by Sul et al. [16]. Generally, it was found that among all the electrolytes (including

H_3PO_4, H_2SO_4, CH_3COOH, and NaOH, $Ca(OH)_2$) the anodic oxide thickness in H_2SO_4 was the highest. Importantly, the oxide formation ability in acidic electrolytes exceeded that in hydroxide solutions. Usually, H_3PO_4 and H_2SO_4 were used to produce thick (tens of microns) and microporous oxide layers at high voltages. In contrast, fluoride solutions were found to have the ability of producing biologically inspired nano-tubular structures in the past few years [17–25]. Due to the importance of nanostructures for biological applications as discussed above, this will be discussed in this section.

The anodization process can be done either at constant voltage (potentiostatic) or constant current (galvanostatic). If the applied voltage exceeds the dielectric breakdown limit of the oxide, the oxide will no longer be resistive to prevent further current flow and oxide growth, which will lead to more gas revolution and sparking. This technique is, thus, known as Anodic Spark Deposition (ASD) or Micro-Arc Oxidation (MAO). For example, it has been reported that the breakdown potentials for H_3PO_4 and H_2SO_4 were around 80 and 100 V, respectively [26]. Below the breakdown limit, the anodic oxide film was relatively thin and usually nonporous using non-fluorine electrolytes.

A constant temperature during the anodization process is usually required to maintain a homogeneous field-enhanced dissolution over the entire area. Since increased temperature will accelerate the chemical dissolution rate, the working temperature is often kept relatively low to prevent the oxide from totally dissolving [26].

2.2.3 Creation of Rough Surfaces

The anodization technique was discovered in the early 1930s and was widely studied in the 1960s to enhance titanium implant osseointegration [27]. These studies usually adopted a high voltage anodization (i.e., ASD) of titanium in electrolyte solutions whose ions would be embedded into the oxide coating, resulting in a microporous structure [27–35]. Table 2.1 shows the anodizing parameters of some ASD studies.

The mechanism of the ASD is usually described by the avalanche theory. During anodization, the newly formed oxide layer on the anode is a dielectric barrier to the current flow and it keeps growing until reaching the dielectric breakdown limit. Generally, the anodized layer is not uniform due to the existence of flaws, defects, local stress, and nonuniform oxide thickness. When the applied voltage increases, the potential drop at the weak points exceeds the dielectric limit so that sparking happens. The local temperature at these points can be up to several thousand Kelvin and lead to a local melting process. Thermal stressing of these anodized titanium leads to the multiplication of weak points, i.e., a cascading process, and

Table 2.1 Experimental parameters of some ASD studies

Electrolyte Composition	Molarity	Voltage (current)	Time (s)	Temperature (°C)	Reference
Sulfuric acid	1	125	–	–	Zinger et al. [28]
	0.5, 1, 3	90, 155, 180	–	–	Yang et al. [29]
Acetic acid	1	80	–	RT	Larsson et al. [30]
	0.1	40–80	8–67	17	Sul et al. [16]
Phosphoric acid	2	175	–	25	Zinger et al. [28]
	0.2	200, 300, 350 (70 A/cm^2)	–	20	Zhu et al. [31]
	1	40–80	10–47	17	Sul et al. [16]
Sodium tripolyphosphate	0.15	(210 A/cm^2)	–	–	Chiesa et al. [27]
Sodium hydroxide	5	10–20	–	25	Huang et al. [66]
	0.1	40–80	22–110	17	Sul et al. [16]
Calcium hydroxide	0.1	40–80	13–53	17	Sul et al. [16]
Calcium glycerophosphate and calcium acetate	0.02/0.1	(70 A/cm^2)	1530	4.1–4.5	Chiesa et al. [27]
	0.03/0.15	200, 260, 300 (70 A/cm^2)		20	Zhu et al. [31]
	0.15/0.02	190–600	180	–	Li et al. [32]
	0.02/0.15	(70 A/cm^2)	1800	–	Suh et al. [33]
	0.02/0.15	350	1200	20	Son et al. [34]
β-glycerophosphate and sodium acetate	0.06/0.3	250–350 (50 A/cm^2)	–	–	Fini et al. [35]

RT Room temperature

consequently breakdown of the dielectric. Figure 2.1 shows a schematic diagram of porous titanium oxide formation proposed by Choi et al. [26].

Basically, the anodic film growth is determined by a balance between the oxide film formation rate and the oxide dissolution rate given by the nature of the electrolyte. Meanwhile, the nature of the electrolyte is closely connected with other processing parameters such as electrolyte concentration, applied voltage, current density, pH, etc. The explanations in detail could be found elsewhere [16].

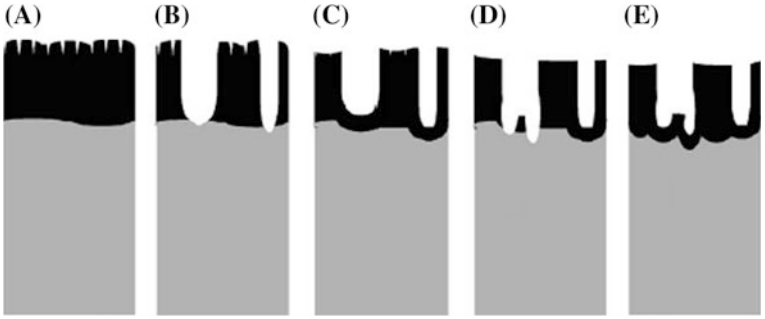

Fig. 2.1 Schematic diagram of porous titanium oxide formation above the breakdown potential: *A* oxide growth to maximal thickness, *B* burst of oxide by the formation of crystallites (pore formation), *C* immediate repassivation of pore tips, *D* burst of repassivated oxide, and *E* dissolution of the formed oxide and second repassivation (adapted from Ref. [26])

2.2.4 Creation of Nano-roughness

While the generation of microstructures through titanium anodization is well-established, current research efforts focus on creating biologically inspired nanometer surface structures. Studies has shown that nanoporous structures can be created by titanium anodization in chromic acid at 10–40 V [36]. Another unique surface morphology obtained through titanium anodization is self-ordered nano-tubular structures [17–25]. For these studies, fluorine electrolyte solutions are used and the applied voltage must be much lower than the dielectric breakdown. Some of the specific anodizing parameters to create titanium nanometer structures are listed in Table 2.2.

The need of fluoride ions to form nanoporous titania structures on a titanium surface under relatively low voltages was first reported by Zwilling et al. [37]. However, the nano-tubular structures were not reported here. In 1999, Grimes and co-workers successfully fabricated self-ordered nanotube arrays after anodizing titanium between 10 and 40 V in dilute (0.5–1.5 wt%) aqueous HF solutions [17]. It was found that the diameters of nanotubes were determined by applied voltage while the final length of tubes were independent of the anodization time.

The tube diameter was approximately 60 nm and tube length was 200 nm at 20 V in 0.5 % HF solution for 20 min (Fig. 2.2). Later, they developed a method to produce tapered, conical-shape titania nanotubes in 0.5 % HF by linearly changing the voltage from 10 to 23 V (Fig. 2.4) [18]. Schmuki and co-workers also observed self-ordered nano-tubular titanium oxide films in HF/H_2SO_4 or CH_3COOH/NH_4F electrolyte solutions [19].

Moreover, the nano-tubular (nano-pore) structure was also achieved in organic electrolytes. Choi et al. used nano-indented titanium for anodization in ethanolic HF and produced a pore lattice with a 500 nm inter-pore distance (Figs. 2.3 and 2.4) [26]. Schmuki's group reported nano-tubular structures using nonaqueous mixtures

Table 2.2 Survey of different fluorine solutions to produce titania nano-tubular structures with different size and thickness

Electrolyte composition (pH)	Voltage (V)	Time (h)	Temperature (°C)	Thickness (nm)	Pore diameter (nm)	Reference
CH_3COOH and 0.5 M HF	10	4	–	60	500 (inter)	Choi et al. [26]
0.5 or 1.5 % HF	10–40	<1	18	250	25–65	Gong et al. [17]
0.5 % HF	10–23	<1	–	300	22–76	Mor et al. [18]
KF and NaF (4.5)	25	20	–	4400	115	Cai et al. [21]
DMSO and CH_3COOH and 4 % HF	20	70	RT	2300	60	Ruan et al. [22]
1 M H_2SO_4 and 0.15 % HF	30	24	–	540	140	Beranek et al. [19]
CH_3COOH and 0.5 % NH_4F	20	1	–	200	30	Tsuchiya et al. [20]
1 M $(NH_4)_2SO4$ and 0.5 % NH_4F	20	–	–	2500	100	Macak et al. [23]
1 M $(NH_4)H_2PO_4$ and 1 M H_3PO_4 and 0.5 % HF	20	40	–	4070	50	Ghicov et al. [24]
0.138 M HF or NaF + 0.5 M H_3PO_4	20	–	24	500	100–120 (outer)	Raja et al. [25]

RT Room temperature

of ethanol and ammonium fluoride without an imprinting treatment [20]. However, in these studies, the depth of titania nanotubes was limited to a few hundred of nanometers. Recently, high-aspect-ratio titania nanotubes up to several micrometers were reported by both Grime's and Schmuki's groups [21–24]. Grime's group reported the formation of 4.4 µm long titania tube arrays by anodizing titanium in NaF or KF of pH 4.5 (Fig. 2.5) [21]. They also reported formation of 2.3 µm thick nano-tubular structures using DMSO/ethanol/HF electrolyte (Fig. 2.6) [22]. Meanwhile, Schmuki's group succeeded in using neutral fluoride solutions to produce nano-tubular structures up to 2.5 µm [23]. They achieved this by controlling the electrochemical parameters to enhance acidification at the bottom of tubes.

Chemical dissolution, field-assisted dissolution, and oxidation are the three main reactions in fluorine electrolyte anodization. Among these, field-enhanced dissolution has been considered as the predominant mechanism of titania tubular structure formation by many researchers [17–24]. The evolution of nanotube

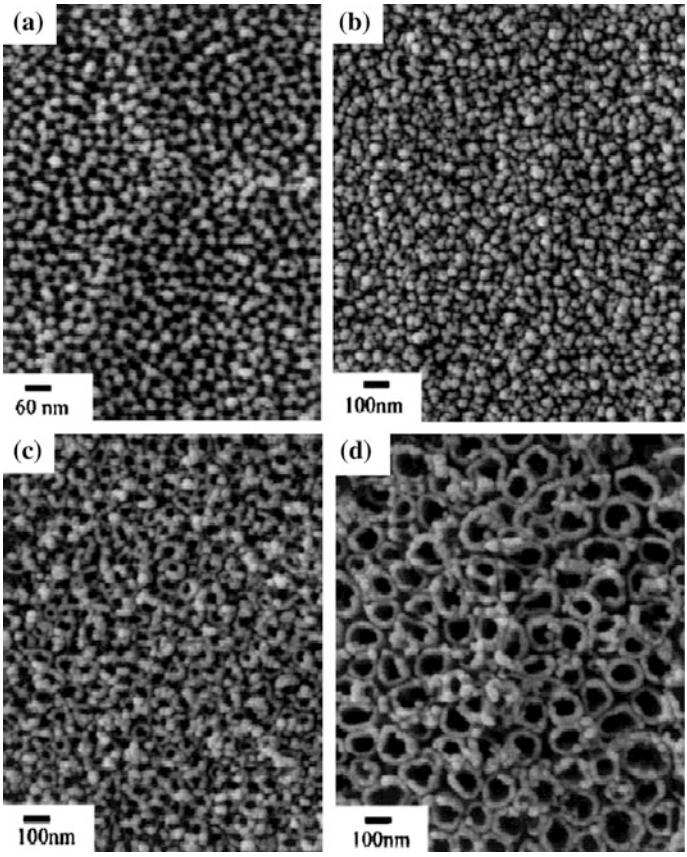

Fig. 2.2 FE-SEM top-view images of porous titanium oxide films anodized in 0.5 wt% HF solution for 20 min under different voltages: **a** 3 V, **b** 5 V, **c** 10 V, and **d** 20 V (adapted from Ref. [17])

structures is shown in Fig. 2.7. Grime and co-workers proposed a mechanism based on a point defect model [18]. Grime proposed that the initial pore formation was due to localized dissolution at weak points and the unanodized metallic portions would exist between the pores. Later, voids were formed in these inter-pore regions by field-enhanced oxidation/dissolution (Fig. 2.8). The growth of voids in equilibrium with the pores would form the final nano-tubular structures. However, it did not explain how voids are created and lead pores to be well-separated, individual tubes. Recently, Raja et al. [25] suggested that the instability of the oxide layer and the self-ordered structures could be explained by the perturbation theory; separation of individual nanotubes of titanium oxide layer from the interconnected nano-pores could be attributed to the repulsion forces of the cation vacancies (Fig. 2.9).

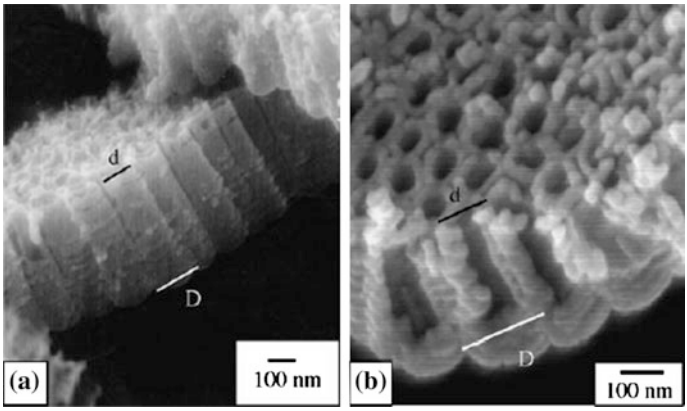

Fig. 2.3 FE-SEM cross-sectional views of the titania nanotubes obtained using a time-varying anodization voltages; *d* denotes diameter of apex and *D* diameter of cone base. **a** Tapered nanotubes obtained using a ramp rate of 0.43 V/min to raise the voltage from 10 to 23 V within 30 min and then holding the voltage at 23 V for 10 min. **b** Tapered nanotubes obtained by initially anodizing the sample at 10 V for 20 min and then increasing the voltage linearly at a rate of 1.0 V/min to 23 V, and finally keeping the voltage at 23 V for 2 min (Ref. [18])

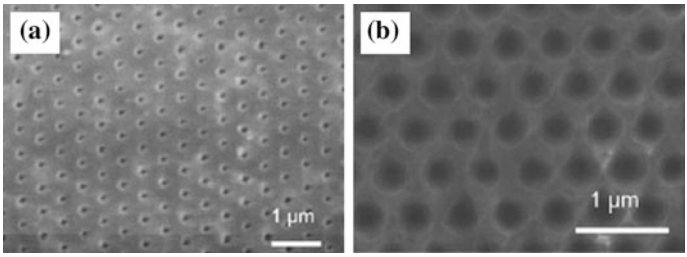

Fig. 2.4 SEM of **a** nano-indented surface of titanium substrate and **b** anodized titanium at 10 V in ethanolic 0.5 M HF for 240 min (adapted from Ref. [26])

2.2.5 Control of Chemical Composition

The ions contained in the electrolyte are usually present in the thick, porous ASD film and the concentration of these elements decreases from the outer layer toward the substrate [31]. For example, phosphorous was found to be embedded in titanium oxide layer after anodization with a H_3PO_4 electrolyte [38]. For electrolytes containing Ca and P, such as calcium glycerophosphate (Ca-GP) and calcium acetate (CA), both Ca and P were contained in the oxide layer with a Ca/P ratio close to HA (1.67) [39]. After an additional hydrothermal treatment (e.g., high pressure streaming), HA crystals were randomly precipitated on the anodic oxide film. These HA crystals were usually columnar or need-like (Fig. 2.10). This could be

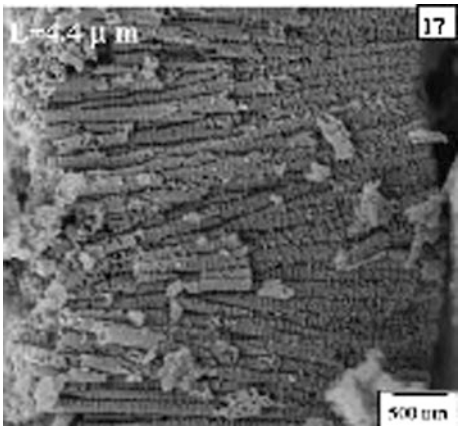

Fig. 2.5 Lateral view of the nanotubes formed in a KF and NaF solution at pH 4.5 under 25 V for 20 h (adapted from Ref. [21])

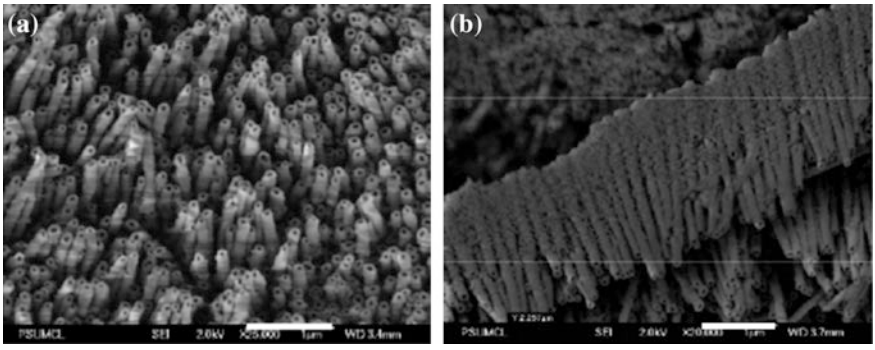

Fig. 2.6 FE-SEM images of titanium foil sample anodized in DMSO and ethanol mixture solution (1:1) containing 4 % HF at 20 V for 70 h. **a** is top-view and **b** is cross-section. Scale bars = 1 μm (adapted and redrawn from Ref. [22])

another way to create HA coatings as opposed to plasma spraying. The advantages of such HA coatings compared to plasma sprayed HA will be discussed in the following sections.

Another approach reported to introduce apatite layers onto the anodized titanium is simply by soaking crystalline titania in simulated body fluid (SBF), because anodized titanium with anatase and rutile titania surfaces were shown to induce apatite formation in vitro. Yang et al. [29] soaked titanium metal in SBF for 6 days after H_2SO_4 anodization and observed uniform apatite formation (Fig. 2.11). One advantage of this method is that the composition and surface morphology of the resulting apatite layer is very close to those in natural bone, but the adhesive strength of such coatings are not clear yet.

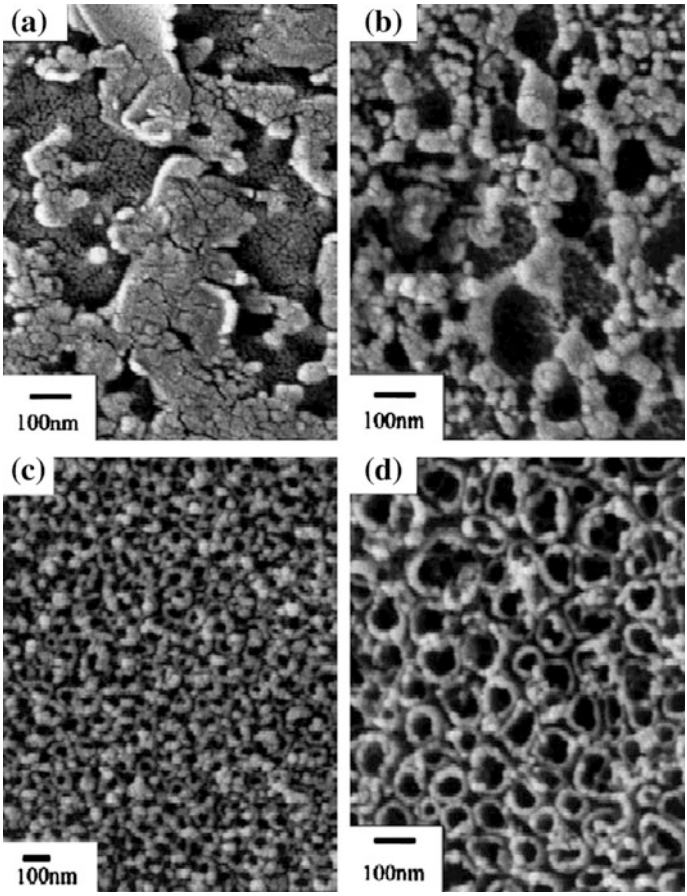

Fig. 2.7 Evolution of nano-tube structures. Porous titanium oxide films anodized in 1.5 % HF at 20 V for **a** 10 s, **b** 30 s, **c** 120 s, and **d** 8 min (adapted from Ref. [17])

Similarly, a two-step procedure was used to produce nanoscale HA for anodized titanium with nano-tubular structures [40]. Specifically, the anodized titanium was treated with NaOH to form nanofibers of bioactive sodium titanate structures on the top edge of the nanotube wall, which was then immersed in a SBF to induce the formation of nanoscale HA (Fig. 2.12). This technique could be useful as well-adherent bioactive nano-HA layers on titanium-based implants are created which simulate the size and shape of natural HA in bone. The advantage of introducing nano-HA onto titanium anodized structures was supported by previous work revealing greater osteoblast functions on nano-HA compared to conventional, or micron grain size, HA [14].

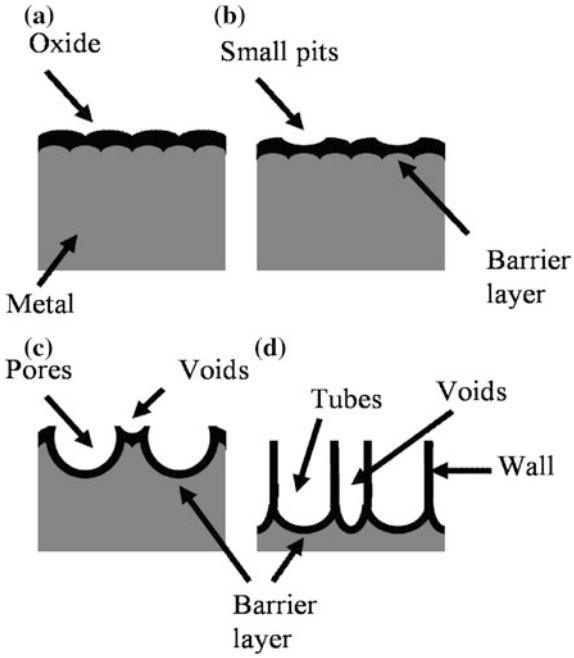

Fig. 2.8 Schematic diagram of the evolution of nano-tube-like structures on the titanium surface during anodization in aqueous HF under constant voltage: **a** oxide formation; **b** pit formation in some concave sites; **c** pore formation and growth under field-enhanced dissolution leading to voids formation; and **d** fully developed tubes (based on the model from Ref. [18] and modified according to experimental observations)

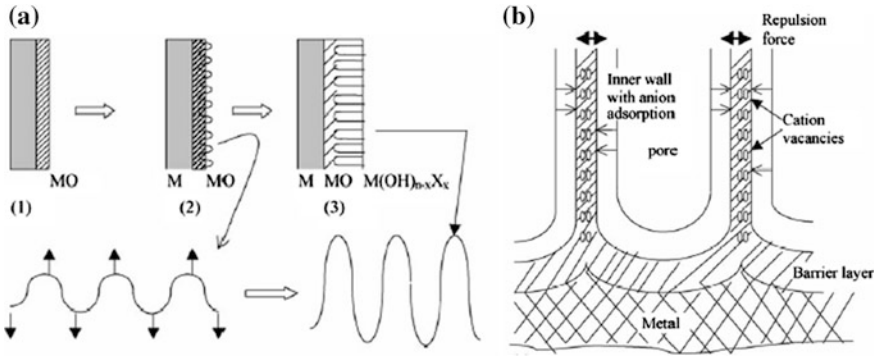

Fig. 2.9 Schematic diagram of **a** pore formation (fluoride addition) during anodization of Ti. The barrier film is intact during porous anodic film formation and substrate metal is not attacked locally. Perturbation of the surface shown in *2* can lead to adsorption of fluorides at the valleys and develop into nano-tubular structure. Higher strain energy density at the valleys drives the mass flow to the lower energy crests; **b** pore separation mechanism. Cation vacancies generated by dissolution of Ti cations are transported radially from the two sides of common wall of the neighbor pores. Charges of similar polarity repel and when electrical neutrality is not maintained this repulsion causes separation of pores into individual nanotubes (adapted and redrawn from Ref. [25])

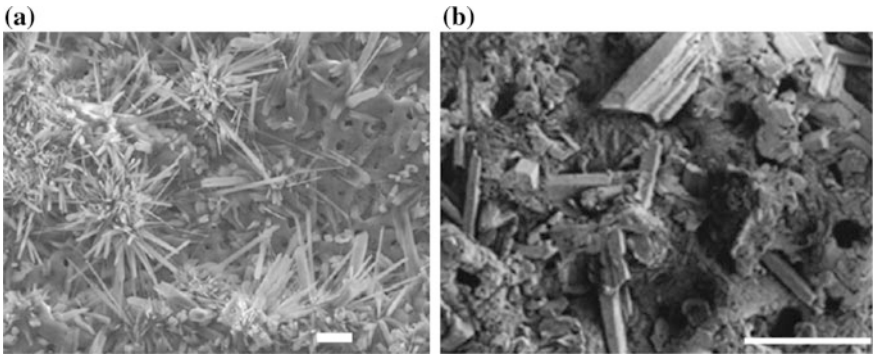

Fig. 2.10 Needle-like or columnar hydroxyapatite crystals deposited on anodized titanium after a hydrothermal treatment. **a** ASD followed by Ishizawa's procedure [43] (adapted and redrawn from reference [27]) and **b** ASD followed by Suh's procedure [33] (adapted and redrawn from Ref. [33]). Scale bars = 10 μm

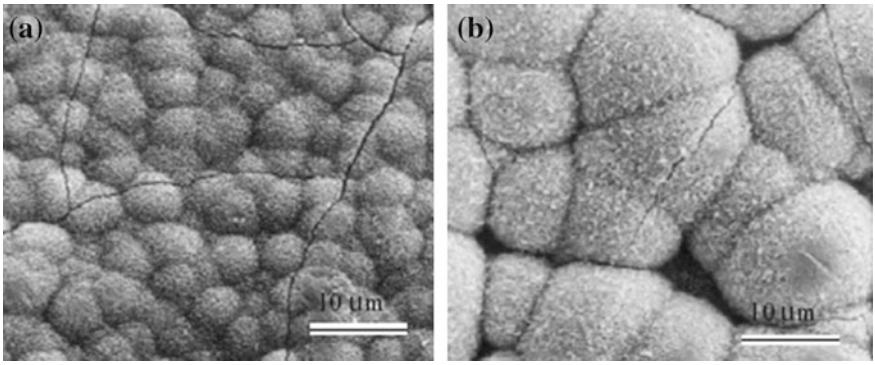

Fig. 2.11 SEM images of titanium metal soaked in SBF for 6 days after they were anodized in 1 M H2SO4 at **a** 155 V and **b** 180 V (adapted and redrawn from Ref. [29])

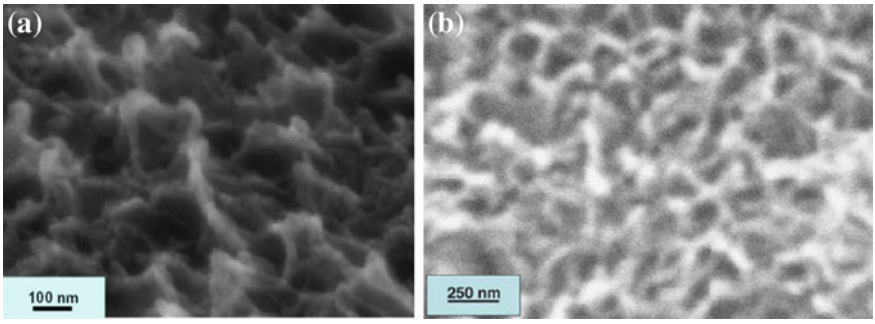

Fig. 2.12 SEM images of **a** nano-inspired sodium titanate nanofibers and **b** nanoscale HA phase (adapted and redrawn from Ref. [40])

2.3 Structure and Properties of Anodized Oxide Film

2.3.1 Structure

The structures and properties of ASD films were widely investigated by Kurze et al. [38]. The typical morphology of the titania layer resulting from ASD is a rough, porous texture with cracks on it (Figs. 2.13 and 2.14). The dimensions of the pores varied from a few hundred nanometers to a few micrometers depending on the processing parameters and are not uniform within the same anodized surface. Moreover, these pores were interconnected and had a layered structure, i.e., they overlapped with each other. The shapes of the pores were mostly round or irregular. The diameter of the pores and the film roughness were reported to increase with greater current densities (Fig. 2.13), [27, 41] applied potential (Fig. 2.14), [29] and electrolyte concentrations [29]. The thickness of oxide film increases with time up to tens of micrometers.

In contrast, the biological-inspired nano-tubular structures were highly ordered. The pore size is determined by the voltage and can be varied from a few tens of nanometers to around 100 nm. The thickness of the tubular-structured oxide was formed to be a few hundred nanometers but has been elongated to a few microns by controlling pH and electrolytes. Generally, the dimensions of nano-tubular structures within one sample are uniform but might be variable due to differences (e.g., surface defects) on a substrate.

2.3.2 Corrosion Resistance and Adhesive Strength

After anodization, thickness of the protective oxide layer increases and it could lead to less ion release in the human body. The oxide barrier layer (the relatively thin,

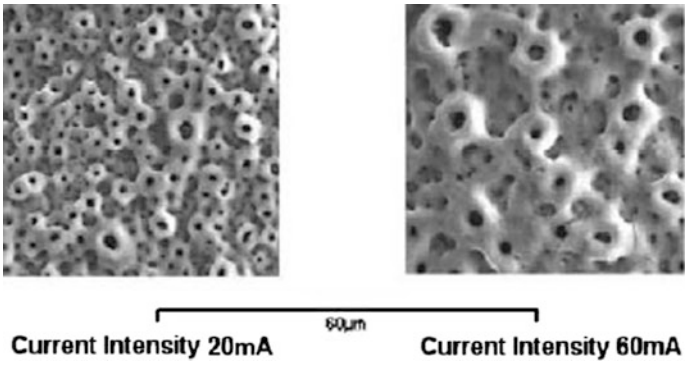

Fig. 2.13 SEM micrographs of an ASD formed film on c.p. grade 2 titanium from an electrolyte containing 0.015 M calcium glycerophosphate and 0.1 M calcium acetate. Increased current density from 20 to 60 mA/cm^2 led to a larger pore size in the ASD porous structure (adapted from Ref. [27])

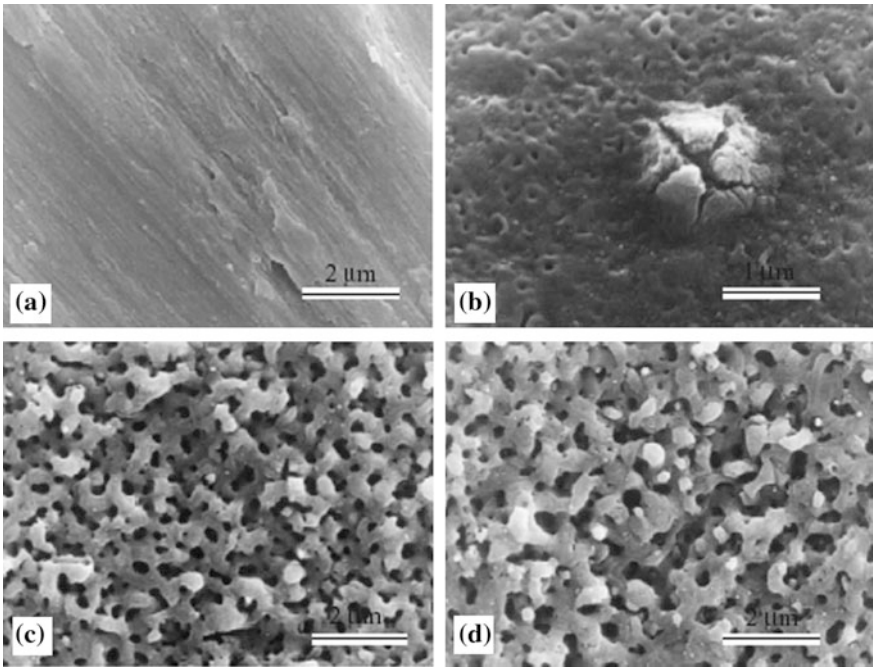

Fig. 2.14 SEM micrographs of ASD formed film on c.p. titanium from an electrolyte containing 1 M H_2SO_4 at voltages of: **a** 0 V, **b** 90 V, **c** 155 V, and **d** 180 V for 1 min. Different voltages from 90 to 155 V led to a larger pore size in the ASD porous structure (adapted from Ref. [29])

nonporous oxide layer under the porous oxide structures) is considered to contribute to the improvement of corrosion resistance. However, it was suggested that the implants' mechanical properties could be impaired with increased spark coating thickness [27].

The interface between the anodic oxide layer and the titanium substrate usually does not show any discontinuity [27]. Besides, the HA crystals on the hydrothermally treated titanium are gradually grown consuming Ca and P in the anodic film. As a result, the interface between the substrate, the anodic film, and the HA film are considerably strong. The adhesive strength between the anodic oxide films and the titanium substrates was reported to be 25 MPa, [42] and the adhesive strength between the oxide/HA coating and the substrate after a hydrothermal treatment was reported to be up to 40 MPa by Ishizawa and Ogino [39, 43] when using less concentrated electrolytes. These values are equivalent or higher than those of plasma sprayed HA onto titanium surfaces, which were reported between 15 and 30 MPa depending on different processing parameters [44, 45]. Moreover, the HA produced from hydrothermal treatment after anodization (AH-HA) seemed to be more stable than plasma sprayed HA (PS-HA). It was reported that the shear strength of PS-HA in SBF decreased from 28.1 to 20.4 MPa after 4 weeks [46]; meanwhile, Ishizawa et al. found that AH-HA retained high durability after

300 days in SBF [39]. So from a mechanical point-of-view, hydrothermally treated anodic titanium would be a better choice than HA plasma sprayed titanium.

2.3.3 Biological Properties of Anodized Titanium

2.3.3.1 In Vitro Studies

Clearly, coating strength, mechanical. and other properties are not the only concern for orthopedic implants. Cytocompatibility leading to promoted bone growth needs to be assessed. Most studies have been reported in vitro bone cell responses to anodized and anodized/hydrothermally treated titanium surface. Fini et al. reported that the adhesion, spreading, proliferation, and differentiation of osteoblast-like cells (HOS-TE85, human osteosarcoma line) were similar on unanodized titanium, titanium anodized enriched with Ca/P, and titanium anodized and hydrothermally treated [35]. An unexpected increase of unattached cells in the latter two substrates was observed. However, the percentage of unattached cells was in the range of 10–20 % which is considered a normal range for cytocompatible materials. On contrast, Rodriguez et al. [47] reported increased osteocalcin production on the anodized and hydrothermally treated titanium surfaces but the highest alkaline phosphate (ALP) activity on control titanium throughout an 8-day study using an osteoblast precursor cell line (ATCC, CRL-1468). Both osteocalcin and ALP are markers of osteoblast differentiation to deposit calcium. They explained that a decrease in ALP activity was in part attributed to the maturation of osteoblast precursor cells and in part attributed to the increased production of mineralized matrix. Also using Ca-GP and CA as an electrolyte, Li et al. reported decreased osteoblastic MG63 cell proliferation when anodization voltage increased above 190 V; however, increased ALP activity of human osteosarcoma cell line was reported with voltages above 300 V [32].

Zhu et al. [31] studied the effects of topography and composition of anodized titanium surfaces on osteoblast (SaOS-2 derived from human osteosarcoma) responses. Their cell experiments showed an absence of cytotoxicity and an increase of cell attachment and proliferation after anodization in an electrolyte composed of Ca-GP and CA. The cells on the surfaces with micropores showed an irregular and polygonal growth and more lamellipodia, while cells on the titanium control showed many thick stress fibers and intense focal contacts. However, they did not find any significant difference for ALP activity. Suh et al. [33] studied the effects of hydrothermally treated anodic films similar to the Zhu formulations and they observed no statistical differences in cell viability using the MTT assay when osteoblasts (ROS 17/2.8, a rat osteosarcoma cell line) were cultured for 4 days on untreated, anodized, and anodized/hydrothermally treated surfaces. In contrast, they found that hydrothermal treatment had an effect on early osteoblast attachment, resulting in a more well-spread shape compared to the cellular rounded shape observed on anodized and control titanium after 6 h (Fig. 2.15).

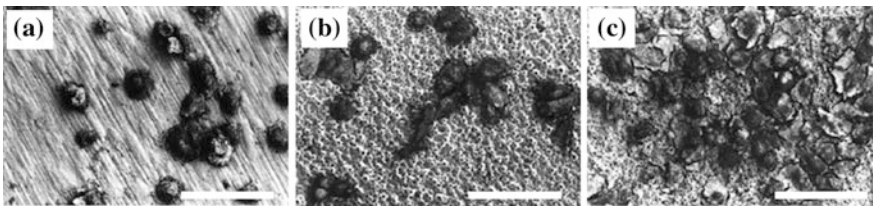

Fig. 2.15 SEM of cells after 6 h culturing on **a** control surface, **b** anodized surface and **c** anodized surface followed by hydrothermal treatment for 4 h. Scale bars = 120 μm (adapted from Ref. [33])

The different observations in the above in vitro studies could be attributed to the use of different anodization parameters and different cell lines. The optimal anodization conditions are still under investigation.

Since the nano-tubular structure is relatively new, few cytocompatibility studies have been completed to examine its potential for use as a novel titanium bone implant surface. However, because of the size and order of the titania tubular structure (which somewhat mimics the natural environment of bone) it is very interesting to determine whether there is any morphological or size advantage of using nano-tubular structures compared to a conventional anodized titanium porous structure for enhancing bone cell functions.

Currently, our research has focused on osteoblast functions on such anodized titanium with nano-tubular titania structures. These structures are similar to those formed by Gong et al. [17]. (0.5 % HF, 20 V, 20 min). After anodization, the tubular structures had increased surface roughness (Fig. 2.16). The inner diameters of the nanotubes were about 70 nm and the depth of them was about 200 nm. To study the effects of nanoroughness and morphology, intermediate samples that possessed a nano-particulate structure and a medium roughness in between the unanodized control and the nano-tubular structure were created (0.5 % HF, 10 V, 20 min) (Fig. 2.16).

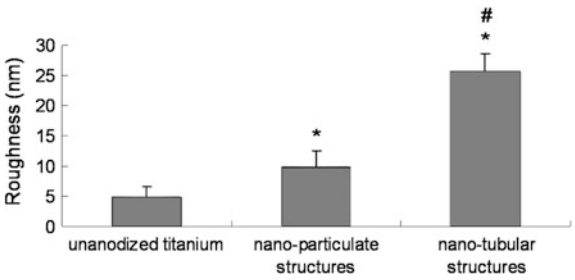

Fig. 2.16 Surface roughness of **a** unanodized titanium, **b** anodized titanium with nano-particulate structures, and **c** anodized titanium with nano-tubular structures. Data = mean ± SEM; n = 3; *p < 0.01 (compared to unanodized titanium) and #p < 0.01 (compared to nano-particulate structure)

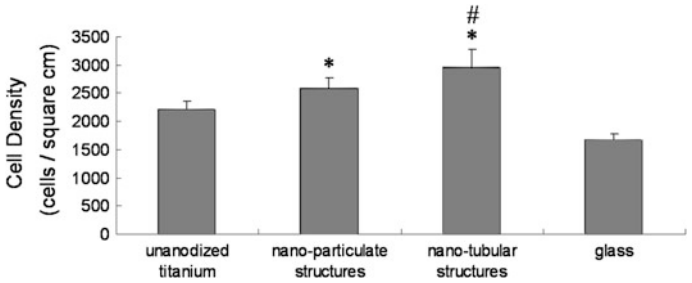

Fig. 2.17 Osteoblast adhesion on unanodized titanium, anodized titanium with nano-particulate structures (10 V, 0.5 % HF, 20 min), anodized titanium with nano-tubular structures (20 V, 0.5 % HF, 20 min), and glass (reference). Values are mean ± SEM; n = 3; *p < 0.1 (compared to unanodized titanium) and #p < 0.1 (compared to anodized titanium with nano-particulate structures)

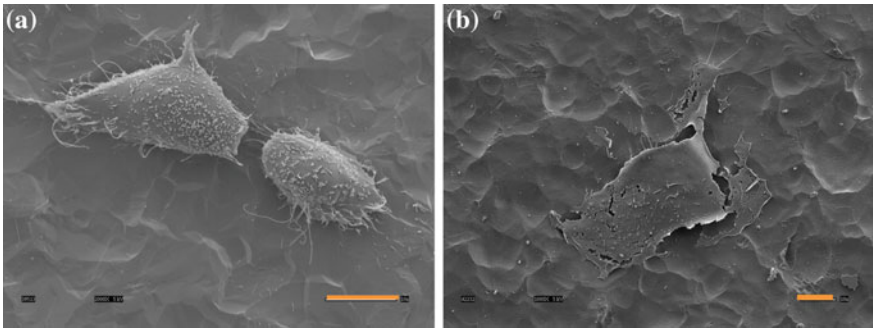

Fig. 2.18 Typical osteoblast morphology on **a** unanodized titanium and **b** anodized titanium surface with nano-tubular structures after 4 h culture. Scale bars = 10 μm

The experiments showed increased osteoblast adhesion after 4 h of culture with greater anodized titanium roughness (Fig. 2.17). The difference in osteoblast morphology was obvious between nano-tubular structures and unanodized titanium. Most cells were well-spread on anodized titanium with nano-tubular structures while they mostly looked round on the control (Fig. 2.18). After 4 weeks of culture, the anodized titanium with nano-tubular structures promoted the highest calcium deposition by osteoblasts among all the samples. These results indicated that the special nano-tubular structures anodized onto the titanium surface may have provided an optimal surface roughness for promoting bone cell function.

2.3.3.2 Mechanisms of Increased Osteoblast Function

Moreover, protein (fibronectin and vitronectin) adsorption on nano-tubular samples has been examined to explore the mechanism of enhanced osteoblast adhesion. Fibronectin and vitronectin are two major proteins that involved in osteoblast

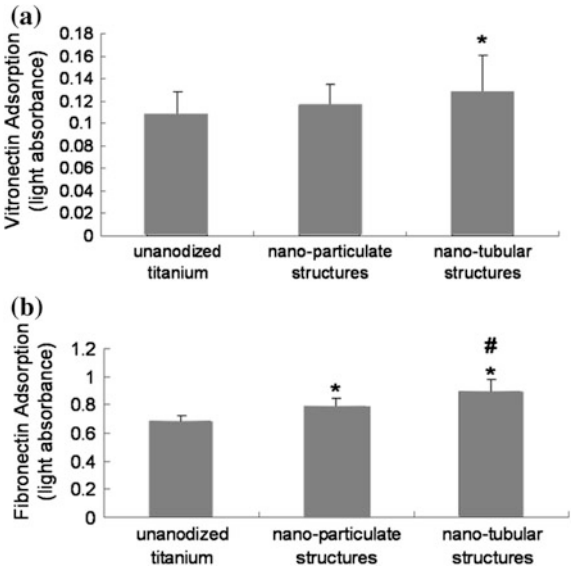

Fig. 2.19 **a** Fibronectin and **b** vitronectin adsorption on unanodized titanium, anodized titanium possessing nano-particulate structures (0.5 % HF, 10 V and 20 min), and anodized titanium possessing nano-tubular structures (0.5 % HF, 20 V and 20 min). Values are mean ± SEM; n = 3; *p < 0.1 (compared to unanodized titanium) and #p < 0.1 (compared to nano-particulate structures)

adhesion [48–50]. Results showed significantly increased both fibronectin (15 %) and vitronectin (18 %) adsorption on nano-tubular structures compared to unanodized titanium samples (Fig. 2.19). Because the cells adhered to the titanium surface via pre-adsorbed proteins, increased fibronectin and vitronectin adsorption on anodized titanium substrates with nano-tubular structures may explain the observed enhanced osteoblast functions.

2.3.3.3 In Vivo Studies

While in vitro assays may generate a quick assessment of cytocompatibility, in vivo studies are necessary to fully evaluate new bone growth. A survey of in vivo investigations of bone tissue reactions to anodized titanium implants is listed in Table 2.3. As with in vitro analysis, the varied oxide properties not only include thickness, but also morphology, chemical composition, crystallinity, and surface roughness.

Some in vivo studies were mainly interested in the effects of thick, porous oxide coating on new bone growth. Less than 200 nm thick oxide film anodized in acetic acid showed no significant difference compared to unanodized samples after implanted into a rabbit 6 weeks [30]. In contrast, a H_3PO_4/H_2SO_4 electrolyte was usually used to form thick anodic films up to tens of microns. Enhanced bone-bonding was found for micron-thick porous anodic oxide films formed in a H_3PO_4/H_2SO_4 electrolyte solution in a rabbit model [51–53].

More importantly, changes of surface chemistry could play a more important role in inducing new bone growth. Several in vivo studies focused on Ca-P enriched anodized titanium with and without hydrothermal treatment [32, 35, 54–57].

Table 2.3 Survey of in vivo investigations of bone tissue reactions to anodized titanium implants

Implant	Treatment	Chemical composition	Oxide thickness (μm)	Oxide/HA morphology (pore size, μm)	Oxide/HA crystallinity	Roughness (μm)	Test	Animal and time (week)	References
cylinder	AO and HT	TiO_2, HA	<10	Porous (1–3)	A + R	ND	Push-out	Rabbits 8	Ishizawa et al. [54]
Screw	E/M and AO	Mainly TiO_2	0.18–0.2	Pores and pits	N	32.3/40.8 nm (rms)	Contact ratio	Rabbits 1, 3, 6	Larsson et al. [30]
Screw	AO	Ti, O, C, P/S	1/10	Porous (1–10)	A + R	1.2 (Sa)	RTQ, RFA	Rabbits 3, 6	Henry et al. [51]
Rod	Ca-P AO w/or w/o HT	Ti, O, Ca/P, HA	5	porous (1–3)/columnar	N/C	1.97 (Ra)	AI	Rats 4, 8	Fini et al. [35]
Screw	Ca-P AO and HT	Ti, O, Ca/P, HA	ND	porous	ND	1.97 (Ra)	AI, push-out strength	Sheep 4, 8, 12	Giavaresi et al. [55, 56]
Screw	Ca-P AO w/or w/o HT	Ti, O, Ca/P, HA	ND	Porous/needle-like	A + R/C	ND	Percent bone contact, RTQ	Rabbits 6,12	Son et al. [57]
Screw	AO	Primary TiO_2	0.2–1	Porous (1.27–2.10)	N, A, A + R	0.96–1.04 (Sa)	RTQ, RFA	Rabbits 6	Sul et al. [52, 53]
Screw	AO	Ti, O, S, P, Ca	1.1–1.3	Porous (<1.5)	A or N	0.82–1.04 (Sa)	RTQ, BMC	Rabbits 6	Sul [59]

Abbreviations: *AO* Anodization, *HT* Hydrothermal treatment, *E* Electropolished, *M* Machined. *C* Crystalline, *N* Noncrystalline, *A* Anatase, *R* Rutile, *RTQ* Removal torque values, *RFA* Resonance frequency analysis, *AI* Affinity index, *BMC* Bone to metal, *ND* Not determined

Ishizawa et al. produced 1–2 μm HA films on anodic oxide layer and compared bone growth on them with unanodized titanium [54]. They found strong bone bonding via push-out tests with anodized titanium after 8 weeks of implantation into rabbits. Following their in vitro work, Fini et al. [35] found the lowest affinity index on anodized titanium while the highest was found on the anodized and hydrothermally treated titanium. The low bone contact on anodized titanium was probably due to the in vivo reduction and degradation of the amorphous titania layer while HA crystals aided bone opposition. Giavaresi et al. [55, 56] also supported the positive role of HA produced from hydrothermal treatment in accelerating bone ingrowth and bone mineralization. Son et al. [57] reported no significant difference for the percent bone contact for all samples but did find significantly increased removal torque strength for anodized implants after 6 weeks of implantation into a rabbit.

The dissolution of AH-HA and PS-HA in vivo was studied by Ishizawa et al. [58]. Basically, the AH-HA was much more durable than PS-HA because of their relatively high crystallinity and their relatively low thickness. Ishizawa et al. also found these two HA had different bone responses [58]. Specifically, new bone thinly spread over the whole AH-HA area while new bone formed from surrounding bones to the PS-HA area. This is probably due to their different degradation properties. One drawback of most of the above studies is that both chemical composition and surface morphology changed after titanium anodization so that it is hard to verify the role of one material property. However, Sul [59] indirectly verified a chemical bonding in vivo by maintaining surface morphology and roughness and changing chemical characteristics (specifically, S, P and Ca enriched implants via anodization).

The removal torque value (RTQ) showed significant differences between Ca-containing anodized titanium implants and unanodized titanium implants as well as S-containing anodized titanium implants and unanodized titanium implants (Fig. 2.20). The bone to metal contact was 186, 232, and 272 % higher in S, P, and Ca implants, respectively, when compared to the control groups. These results

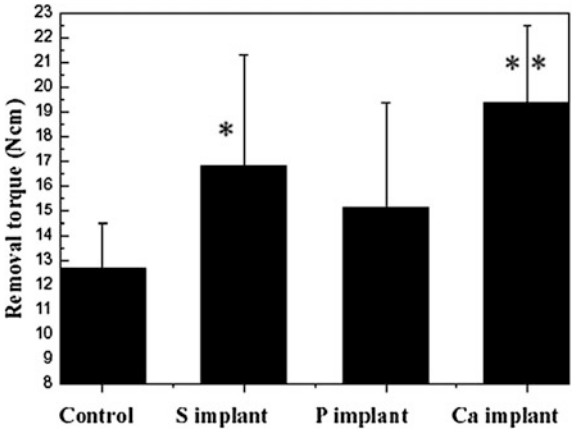

Fig. 2.20 Mean removal torque values after 6 weeks of healing time. *p < 0.05, **p < 0.001 (adapted from Ref. [59])

confirmed that ions incorporated into the titanium oxide layer during anodization could have important roles in enhancing bone juxtaposition.

2.4 Future Directions

As a surface modification method, anodization can lead to desired chemistry and/or topography changes and could be used with other treatments (e.g., hydrothermal) together.

First, anodization provides a controlled way to create nano-roughness or even nano-features. Generally, there are two mechanisms that are responsible for osseointegration of bone: biomechanical interlocking and biological interactions. For biomechanical interlocking, it depends on the roughness, and surface irregularity. Current femoral stems made of titanium alloys are usually macro-textured to provide such surface features for bone to mechanically interlock. For biological interactions, it involves complex systems. Considering roughness in different scales, it is reported that increased micro/submicron-roughness could enhance bone cell function, such as ALP activity [60, 61] while some other studies have revealed the enhanced cell-implant interactions on nanoporous or nanophase materials [14, 15, 62, 63]. Ideally, the future titanium implant should possess roughness in all three scales: macro, micro, and nano. One possible approach to accomplish this is by subjecting implants to techniques like polishing and mechanical grinding that promote micro-roughness, and then to induce nano-tubular structures by a quick anodization process.

Second, micro/nano HA films produced using anodized titanium shows some advantages over conventional ones. Although plasma spray is still widely used for HA coatings on titanium, anodization has a strong role to play to incorporate Ca and P into Ti coatings. For example, anodization has the ability to form uniform and thin HA or calcium phosphate layers on titanium implants of various shapes. Moreover, HA deposited onto the anodized titanium could be nanoscale in dimension. One problem that still needs to be more fully investigated is the bonding strength between apatite crystals and the anodic oxide.

Furthermore, anodization can be used to incorporate drug delivery into titanium-based implants to enhance new bone formation. Porous ASD surfaces could be used as matrices for drug storage and release [64]; similarly, the nano-tubular structures could serve as reservoirs of chemical mediators, such as bone morphogenetic protein-2 (BMP-2) and osteogenic protein-1 (OP-1, BMP-7) [65]. In the future, studies should concentrate on embedding these growth factors into the unique porosity that can be well controlled on titanium for orthopedic applications.

In a word, anodization as a quick and efficient modification method of titanium based implants shows significant promise for enhancing their 10–15-year lifetime.

Acknowledgments The authors would like to thank National Science Foundation Nanoscale Exploratory Research Grant for financial assistance.

References

1. Brunette, D. M, Tengvall, P., Textor, M., & Thomsen, P. (2001). *Titanium in medicine* (p. 171). Berlin: Springer.
2. Shackelford, J. F. (1999). *Bioceramics* (vol. 1, p. 17). Netherlands: Gordon and Breach Science Publishers.
3. Moran, C. G., & Horton, T. C. (2000). *BMJ, 320*, 820.
4. Brunette, D. M., Tengvall, P., Textor, M., & Thomsen, P. (2001). *Titanium in medicine* (p. 232). Berlin: Springer.
5. Larsson, C., Thomsen, P., Aronsson, B. O., Rodahl, M., Lausmaa, J., Kasemo, B., & Ericson, L. E. (1996). *Biomaterials, 17*, 605.
6. Kim, H. M., Miyaji, F., Kokubo, T., & Nakamura, T. (1997). *Journal of Materials Science: Materials in Medicine, 8*, 341.
7. Kokubo, T., Kim, H. M., Kawashita, M., & Nakamura, T. (2004). *Journal of Materials Science: Materials in Medicine, 15*, 899.
8. Sittig, C., Textor, M., Spencer, N. D., Wieland, M., & Vallotton, P. H.: *Journal of Materials Science: Materials in Medicine, 10*, 35.
9. Bordji, K., Jouzeau, J. Y., Mainard, D., Payan, E., Netter, P., Rie, K. T., et al. (1996). *Biomaterials, 17*, 929.
10. Furlong, R., & Osborn, J. F. (2001). *Journal of Bone and Joint Surgery, 73B*, 741.
11. Kim,S.-S., Park, M. S., Jeon, O., Choi, C. Y., & Kim, B.-S. *Biomaterials* (in press).
12. Baker, K. C., Anderson, M. A., Oehlke, S. A., Astashkina, A. I., Haikio, D. C., Drelich, J., et al. *Growth, Materials Science and Engineering: C* (in press).
13. Sato, M., Slamovich, E. B., & Webster, T. J. (2005). *Biomaterials, 26*, 349.
14. Bronzino, J. D. (1995). *Biomedical engineering handbook* (p. 274). Boca Raton: CRC Press.
15. Webster, T. J., & Ejiofor, J. U. (2004). *Biomaterials, 25*, 4731.
16. Sul, Y. T., Johansson, C. B., Jeong, Y., & Albrektsson, T. (2001). *Medical Engineering and Physics, 23*, 329.
17. Gong, D., Grimes, C. A., Varghese, O. K., Hu, W., Singh, R. S., Chen, Z., & Dickey, E. C. (2001). *Journal of Materials Research, 16*, 3331.
18. Mor, G. K., Varghese, O. K., Paulose, M., Mukherjee, N., & Grimesa, C. A. (2003). *Journal of Materials Research, 18*, 2588.
19. Beranek, R., Hildebrand, H., & Schmuki, P. (2003). *Electrochemical and Solid-State Letters, 6*, B12.
20. Tsuchiya, H., Macak, J. M., Taveira, L., Balaur, E., Ghicov, A., Sirotna, K., & Schmuki, P. (2005). *Electrochemistry Communications, 7*, 576.
21. Cai, Q., Paulose, M., Varghese, O. K., & Grimes, C. A. (2005). *Journal of Materials Research, 20*, 230.
22. Ruan, C., Paulose, M., Varghese, O. K., Mor, G. K., & Grimes, C. A. (2005). *The Journal of Physical Chemistry B, 109*, 15754.
23. Macak, J. M., Tsuchiya, H., & Schmuki, P. (2005). *Angewandte Chemie International Edition, 44*, 2100.
24. Ghicov, A., Tsuchiya, H., Macak, J. M., & Schmuki, P. (2005). *Electrochemistry Communications, 7*, 505.
25. Raja, K. S., Misra, M., & Paramguru, K. (2005). *Electrochimica Acta, 51*, 154.
26. Choi, J., Wehrspohn, R. B., Lee, J., & Gosele, U. (2004). *Electrochimica Acta, 49*, 2645.
27. Chiesa, R., Sandrini, E., Santin, M., Rondelli, G., & Cigada, A. (2003). *Journal of Applied Biomaterials and Biomechanics, 1*, 91.
28. Zinger, O., Chauvy, P. F., & Landolt, D. (2003). *Journal of the Electrochemical Society, 150*, 495.
29. Yang, B., Uchida, M., Kim, H.-M., Zhang, X., & Kokubo, T. (2004). *Biomaterials, 25*, 1003.
30. Larsson, C., Thomsen, P., Aronsson, B.-O., Rodahl, M., Lausmaa, J., Kasemo, B., & Ericson, L. E. (1996). *Biomaterials, 17*, 605.

31. Zhu, X., Chen, J., Scheideler, L., Reichl, R., & Geis-Gerstorfer, J. (2004). *Biomaterials, 25*, 4087.
32. Li, L. H., Kong, Y. M., Kim, H. W., Kim, Y. W., Kim, H. E., Heo, S. J., & Koak, J. Y. (2004). *Biomaterials, 25*, 2867.
33. Suh, J. Y., Jang, B. C., Zhu, X., Ong, J. L., & Kim, K. (2003). *Biomaterials, 24*, 347.
34. Son, W. W., Zhu, X., Shin, H. I., Ong, J. L., & Kim, K. H. (2003). *Journal of Biomedical Materials Research Part B: Applied Biomaterials, 66B*, 520.
35. Fini, M., Cigada, A., Rondelli, G., Chiesa, R., Giardino, R., Giavaresi, G., et al. (1999). *Biomaterials, 20*, 1587.
36. Baun, W. L. (1980). *Surface Technology, 11*, 421.
37. Zwilling, V., Darque-Ceretti, E., Boutry-Forveille, A., David, D., Perrin, M. Y., & Aucouturier, M. (1999). *Surface and Interface Analysis, 27*, 629.
38. Kurze, P., Krysmann, W., & Schneider, H. G. (1986). *Crystal Research and Technology, 21*, 1603.
39. Ishizawa, H., & Ogino, M. (1995). *Journal of Biomedical Materials Research, 29*, 1071.
40. Oh, S.-H., Finõnes, R. R., Daraio, C., Chen, L.-H., & Jin, S. (2005). *Biomaterials, 26*, 4938.
41. Delplancke, J. L., & Winand, R. (1973). *Electrochimica Acta, 33*, 1539.
42. Schreckenback, J. P., Marx, G., Schlottig, F., Textor, M., & Spencer, N. D. (1999). Journal of Surface Science. *Materials in Medicine, 10*, 453.
43. Ishizawa, H., & Ogino, M. (1995). *Journal of Biomedical Materials Research, 29*, 65.
44. Lu, Y. P., Zhu, R. F., Li, S. T., Song, Y. J., Li, M. S., & Lei, T. Q. (2003). *Materials Science and Technology, 19*, 260.
45. Yang, Y., & Ong, J. L. (2003). *Journal of Biomedical Materials Research Part A, 64*, 509.
46. Yang, Y. C., Chang, E., & Lee, S. Y. (2003). *Journal of Biomedical Materials Research Part A, 67*, 886.
47. Rodriguez, R., Kim, K., & Ong, J. L. (2003). *Journal of Biomedical Materials Research Part A, 65*, 352.
48. Anselme, K. (2000). *Biomaterials, 21*, 667.
49. Hayman, E. G., Pierschbacher, M. D., Suzuki, S., & Ruoslahti, E. (1985). *Experimental Cell Research, 160*, 245.
50. Thomas, C. H., McFarland, C. D., Jenkins, M. L., Rezania, A., Steel, J. C., & Healy, K. E. (1997). *Journal of Biomedical Materials Research, 37*, 81.
51. Henry, P., Tan, A. E., & Allan, B. P. (2000). *Applied Osseointegration Research, 1*, 15.
52. Sul, Y. T., Johansson, C. B., Jeong, Y., Wennerberg, A., & Albrektsson, T. (2002). *Clinical Oral Implants Research, 13*, 252.
53. Sul, Y. T., Johansson, C. B., Roser, K., & Albrektsson, T. (2002). *Biomaterials, 23*, 1809.
54. Ishizawa, H., Fugino, M., & Ogino, M. (1995). *Journal of Biomedical Materials Research, 29*, 1459.
55. Giavaresi, G., Fini, M., & Cigada, A. (2003). *Biomaterials, 24*, 1583.
56. Giavaresi, G., Fini, M., Cigada, A., Chiesa, R., Rondelli, G., Rimondini, L., et al. (2003). *Journal of Biomedical Materials Research Part A, 67*, 112.
57. Son, W. W., Zhu, X., Shin, H. I., Ong, J. L., & Kim, K. H. (2003). *Journal of Biomedical Materials Research. Part B, Applied Biomaterials, 66B*, 520.
58. Ishizawa, H., Fujino, M., & Ogino, M. (1997). *Journal of Biomedical Materials Research, 35*, 199.
59. Sul, Y. T. (2003). *Biomaterials, 24*, 3893.
60. Feng, B., Wang, J., Yang, B. C., Qu, S. X., & Zhang, X. D. (2003). *Biomaterials, 24*, 4664.
61. Boyan, B. D., Batzer, R., Kiesewetter, K., Lie, Y., Cochran, D. L., Szmuckler-Moncler, S., et al. (1998). *Journal of Biomedical Materials Research, 39*, 77.
62. Karlsson, M., Palsgard, E., Wilshaw, P. R., & Silvio, L. D. (2003). *Biomaterials, 24*, 3039.
63. Webster, T. J., Ergun, C., Doremus, R. H., Siegel, R. W., & Bizios, R. (2001). *Biomaterials, 22*, 1327.

64. Dunn, D. S., Raghaven, S., & Volz, R. G. (1994). *Journal of Applied Biomaterials, 5*, 325.
65. Varkey, M., Gittens, S. A., & Uludag, H. (2004). *Expert Opinion on Drug Delivery, 1*, 19.
66. Huang, H.-H., Pan, S.-J., Lai, Y.-L., Lee, T.-H., Chen, C.-C., & Lu, F.-H. (2004). *Scripta Materialia, 51*, 1017.

http://www.springer.com/978-3-319-33487-5

Surgical Tools and Medical Devices
Ahmed, W.; Jackson, M.J. (Eds.)
2016, XX, 691 p. 381 illus., 161 illus. in color.,
Hardcover
ISBN: 978-3-319-33487-5